JOURNAL OF GEOPHYSICAL RESEARCH, VOL. 113, D14309, doi:10.1029/2007JD009575, 2008

Relationship of loss, mean age of air and the distribution of CFCs to stratospheric circulation and implications for atmospheric lifetimes

A. R. Douglass,[1] R. S. Stolarski,[1] M. R. Schoeberl,[1] C. H. Jackman,[1] M. L. Gupta,[1,4] P. A. Newman,[1] J. E. Nielsen,[2,3] and E. L. Fleming[3]

Received 15 November 2007; revised 17 February 2008; accepted 29 February 2008; published 24 July 2008.

[1] Projections of the recovery of the ozone layer are made with global atmospheric models using a specified time series of mixing ratios of ozone depleting substances (ODSs) at the lower boundary. This time series is calculated using atmospheric mixing ratio observations, emission rates, and an estimate for the atmospheric lifetime. ODS destruction and simulated atmospheric-lifetime vary among models because they depend on the simulated stratospheric transport and mixing. We investigate the balance between the annual change in ODS burden, its atmospheric loss, and the annual ODS input to the atmosphere using several models. Some models produce realistic distributions for the mean age of air and some do not. Back trajectory calculations relate the fractional release (one minus the amount of ODS at a location relative to its stratospheric entry value) to the mean age through the age spectrum, showing that, for the individual spectrum elements, the maximum altitude and loss increase with age. Models with faster circulations produce "young" distributions for the age of air and fail to reproduce the observed relationship between the mean age of air and the fractional release. Models with realistic mean age of air reproduce the observed relationship. These models yield a lifetime for $CFCl_3$ of ~56 years, longer than the 45 year lifetime currently used to project future mixing ratios. Use of flux boundary conditions in assessment models would have several advantages, including consistency between the ODS evolution and simulated loss even if the simulated residual circulation changes due to climate change.

Citation: Douglass, A. R., R. S. Stolarski, M. R. Schoeberl, C. H. Jackman, M. L. Gupta, P. A. Newman, J. E. Nielsen, and E. L. Fleming (2008), Relationship of loss, mean age of air and the distribution of CFCs to stratospheric circulation and implications for atmospheric lifetimes, *J. Geophys. Res.*, *113*, D14309, doi:10.1029/2007JD009575.

1. Introduction

[2] Current ozone assessment efforts have several goals. One is to verify that the ozone decreases of the 1980s and 1990s have ceased. Another is to predict the behavior of the ozone layer, as the atmospheric burden of greenhouse gases increases and the concentrations of chlorofluorocarbons (CFCs) decline. The CFC decline is due to a substantial reduction of emission and continued atmospheric loss mainly through photolysis by ultraviolet radiation in the stratosphere (e.g., Chapter 8 of *Scientific Assessment of Ozone Depletion: 2006* (*WMO* [2007], hereafter referred to as WMO2007). This paper is related to the second goal, and examines the consistency between the annual change in the integrated atmospheric amount, the computed atmospheric loss and the input of CFCs to the atmosphere implied by the boundary conditions.

[3] The procedures used to produce the time series of CFC mixing ratios that are used in assessments are discussed in detail in Chapter 8 of WMO2007. The atmospheric lifetimes used to project the future mixing ratios are assessed in Chapter 1 of the same report. These boundary conditions, specified at the lowest model layer, largely control the time evolution of the atmospheric burden of the source gases (i.e., the total mass of the source gas in the atmosphere) in all assessment models because the variations of the mass of source gases in the stratosphere among the models are small compared with the mass of the source gas in the troposphere. Projections for the recovery of the ozone hole using semiempirical models also rely on these predicted mixing ratios for chlorine and bromine source gases [e.g., *Newman et al.*, 2006].

[4] Mixing ratio boundary conditions have been used in assessments since the late1980s. Prior assessments predated international agreements to control CFC production, and used a combination of emissions and mixing ratios to focus on the ozone change in the upper atmosphere (e.g., *Atmospheric Ozone 1985: Assessment of our Understanding of the Processes Controlling its present Distribution and*

[1] Atmospheric Chemistry and Dynamics Branch, NASA Goddard Space Flight Center, Greenbelt, Maryland, USA.
[2] Global Modeling and Assimilation Office, NASA Goddard Space Flight Center, Greenbelt, Maryland, USA.
[3] Science Systems and Applications, Inc., NASA Goddard Space Flight Center, Greenbelt, Maryland, USA.
[4] Now at Federal Aviation Administration, Washington, DC, USA.

0148-0227/08/2007JD009575$09.00

Change, [*WMO*, 1985]). In contemporary assessment calculations the mixing ratio boundary conditions largely control the evolution of the mixing ratios of Cl_y (total inorganic chlorine) and its components in the upper stratosphere where nearly all the CFCs have been destroyed. The time evolution of Cl_y depends slightly on the circulation. For example, a more rapid overturning stratospheric circulation will produce a peak in Cl_y a year or two ahead of a slower circulation.

[5] The dependence on the circulation is apparent in the distributions of CFCs and Cl_y in the lower stratosphere. *Waugh et al.* [2007] use CTM simulations using different meteorological fields, horizontal resolution and upper boundary height to show how differences in simulated transport and mixing affect the net destruction of the source gases and the distributions of Cl_y. The models shown in Figure 6.8 of WMO2007 use the same boundary conditions, yet the peak October zonal mean inorganic chlorine (Cl_y) at 50 hPa 80°S exhibits a spread of about 0.75 ppbv (~25%) ignoring outliers.

[6] Despite the difference in the peak amounts of Cl_y, its evolution over time is similar among most of the models. In the WMO2007 models Cl_y increases substantially between 1980 and 2000, and decreases by a similar amount between 2005 and about 2050 in direct response to the imposed mixing ratio boundary conditions. Here we show that the constraint on the overall temporal evolution of the CFCs at the surface and Cl_y in the upper stratosphere produces inconsistency between the annual change in burden (prescribed by the boundary conditions) and the simulated loss.

[7] In addition to their use in predicting the future mixing ratios of CFCs, atmospheric lifetimes are important for some methods used to evaluate the reservoirs of CFCs called banks. Banks exist because CFCs have commonly been used in closed applications such as foams, refrigeration and air conditioning. As long as the appliances remain operational, the CFCs are sealed and not released to the atmosphere. The magnitude and rate of release of CFCs from these banks are subjects of debate. A "top down" estimate of a bank is the cumulative difference of estimated production (based on production and sales data) and the emissions (inferred from atmospheric observations using a model and a presumed lifetime). "Bottom-up" bank estimates rely on a detailed analysis of applications that involve long-term containment of CFCs [*McCulloch et al.*, 2001, 2003]. The top-down analysis was used by *Scientific Assessment of Ozone Depletion: 1998* [*WMO*, 1999] and *Scientific Assessment of Ozone Depletion: 2002* [*WMO*, 2003]. The bottom-up analysis is used by *Special Report: Safeguarding the ozone layer and the global climate system: Issues related to hydrofluorcarbons and perfluorocarbons* [*IPCC*, 2005]. *Daniel et al.* [2007] analyze the banks computed from a "top down" analysis versus those computed from a bottom-up analysis. The maximum annual global emissions of chlorofluorocarbons (CFCs) took place during the late 1980s around the same time as the international agreements to ban production (~350 Ktons/a for $CFCl_3$ and ~460 Ktons/a for CF_2Cl_2). These are far greater than estimates of emissions from banks, but the emissions from the banks are presently comparable to annual atmospheric loss estimates and differences in the bank estimates are significant for decadal predictions. *Daniel et al.* [2007] point out that even small errors in lifetime accumulate, leading to uncertainty in the top-down bank estimates and also show that differences in bank estimates are large enough to impact predictions for future levels of CFCs and ozone recovery.

[8] The purpose of this paper is to use a variety of model simulations to investigate the relationships among the atmospheric burden, the lifetime and the loss rates of CFCs. In addition to global model simulations, we use back trajectory calculations to produce an age spectrum in order to relate the mean age and fractional release. We present results from models that produce both realistic and unrealistic distributions for the stratospheric age-of-air. We show that the lower stratospheric relationships between the fractional release of chlorine from $CFCl_3$ and CF_2Cl_2 and the age-of-air produced by simulations with realistic age-of-air are in better agreement with relationships derived from aircraft observations by *Schauffler et al.* [2003]. Models with faster circulations do not produce realistic age-of-air and also do not reproduce the observed relationship between fractional release and mean age. In all simulations the annual change in atmospheric burden is specified by the mixing ratio boundary conditions and is thus disconnected from the simulation loss. The fluxes are free to obtain any value as determined by interior transport and loss rates. In simulations with "young" age-of-air the CFC lifetime is equal to or shorter than that presumed in WMO2007 and the inferred boundary flux of CFCs can be unrealistically large in the early part of the present century. In simulations with realistic age-of-air, the lifetime is longer than presumed in WMO2007 and the inferred boundary flux of CFCs is negative after about 2010. The negative flux is computed because the annual decrease in atmospheric burden imposed by the boundary conditions exceeds the simulated loss.

[9] The models used in this analysis are described in the following section. Simulation results are presented in section 3. In section 4 we build on the results of *Hall* [2000] and *Schoeberl et al.* [2000], using trajectory simulations of age spectra and annual stratospheric loss rates to explain the relationship between the mean age-of-air and the fractional release of CFCs. The implications of the comparisons with observations for determination of CFC lifetime and removal from the atmosphere are discussed in section 5. We also consider the possibility that a speed-up in the Brewer Dobson Circulation due to climate change will impact the annual CFC loss and thus the ozone recovery [e.g., *Butchart and Scaife*, 2001]. Conclusions follow in section 6.

2. Model Descriptions

[10] Two types of atmospheric numerical models are used to predict the response of ozone to changes in the composition and climate of the atmosphere. A chemistry/climate model (CCM) combines a representation of photochemical processes with a general circulation model (GCM). In a CCM, ozone and other radiatively active gases are transported by the simulation winds, and the computed constituent fields are used to compute net radiative heating rates for the GCM, ensuring consistency among dynamics, radiation and photochemistry. A chemistry transport model (CTM) differs from a CCM in that the meteorological information needed for constituent transport and to account for temperature dependence of photochemical processes is input to the model from an external source such as a

Table 1. Summary of the Simulations Used in This Work[a]

Model	Duration	Realistic Age of Air
2D-base	1935–2099	yes
2D-fast	1935–2099	no
GMI-GCM	1995–2030	yes
GMI-DAS	1995–2030	no
CGCM		
P1 SST1	1950–2004	yes
P2 SST1	1950–2004	yes
F1 SST2	1996–2099	yes
F2 SST2	1971–2049	yes
F3 SST3	1971–2052	yes
F4 SST3	2000–2099	yes

[a]For CGCM simulations "P" refers to past simulations and "F" refers to future simulations. The sea surface temperature and ice distributions are denoted by SST (observed (Hadley)), SST (Modeled HadGEM1) and SST3 (Modeled NCAR CCM3). References are given in the text.

GCM or a data assimilation system. CTMs may be three-dimensional or two-dimensional (latitude/altitude) but heating rates that would be calculated from trace gas distributions in CTMs are not necessarily consistent with the input meteorological fields.

[11] The surface mixing ratio boundary conditions for source gases including chlorofluorocarbons are specified for all simulations following scenario AB of the *Scientific Assessment of Ozone Depletion: 2002* [*WMO*, 2003]. Scenario AB was also used in the modeling studies presented in WMO2007. Another scenario, A1, presented in Table 8-5 of WMO2007 is virtually the same as scenario AB up to 2010. Although there are differences between scenarios AB and A1 after 2010, these will not impact the results of this study. The models used for these multidecadal simulations are described below; the simulations are summarized in Table 1.

[12] We also use a trajectory approach described by *Schoeberl et al.* [2000] to produce age spectra and to interpret the relationship between the mean age of air and the constituent distributions. The trajectory model is summarized after descriptions of the CCM and the CTMs.

2.1. GEOS-4 CCM

[13] The Goddard CCM, described briefly by *Stolarski et al.* [2006a], combines the GEOS-4 GCM (Goddard Earth Observing System, Version 4, General Circulation Model) with a representation of stratospheric photochemistry. Here we refer to this model as CGCM. *Pawson et al.* [2008] describe CGCM and its performance. The GCM dynamical core uses a flux form semi-Lagrangian transport scheme [*Lin and Rood*, 1996, 1997] and a quasi-Lagrangian vertical coordinate system [*Lin*, 1997] to ensure accurate representation of the transport by the resolved-scale flow. The *Lin and Rood* [1996] transport scheme is also used for constituent advection. The photochemical mechanism includes all photolytic, gas phase and heterogeneous reactions thought to be of importance in the stratosphere. The photochemical scheme, an updated version of that used in the Goddard CTM [e.g., *Douglass and Kawa*, 1999, and references therein] uses family approximations and has been extensively tested through applications of the Goddard CTM [*Douglass et al.*, 2001; *Stolarski et al.*, 2006b]. Reaction rate and cross section data are taken from the Jet Propulsion Laboratory Evaluation 14 [*Sander et al.*, 2003]. Processes involving polar stratospheric clouds use the parameterization described by *Considine et al.* [2000]. In the troposphere ozone relaxes to the climatology described by *Logan* [1999]. The ozone simulated using the CTM with meteorological fields from the GCM was shown to compare well with the ozone climatology used in the GCM before attempting to couple the GCM and photochemistry. The spatial resolution for simulations presented here is 2° latitude by 2.5° longitude with 55 layers from the surface to 0.01 hPa. A clock tracer is included in the simulation, providing information about the three-dimensional distribution of the mean age of air but no information about the age spectrum.

[14] The Brewer Dobson circulation in the CGCM is shown to be realistic by comparisons with observations showing the rate of ascent of tropical moisture anomalies and the decrease of the amplitude of the anomalies with height [*Eyring et al.*, 2006]. A weakness of the CGCM, common among CCMs, is that its south polar vortex lasts several weeks longer than is consistent with observations [*Eyring et al.*, 2006; *Pawson et al.*, 2008]. This deficiency will have minimal impact on the computed CFC lifetime. The CGCM simulations used in this work differ in duration, and source of sea surface temperatures (SST) and sea-ice distributions at the lower boundary. Past simulations (1950–2004 use the "HadISST" (Hadley Center Ice and Sea-Surface Temperature) data set of *Rayner et al.* [2003]. Future simulations are integrated until 2049 or later, and use output from coupled ocean-atmosphere model simulations: HadGem1 [*Johns et al.*, 2006] and NCAR CCSM3 [*Kiehl et al.*, 1998]. The duration of the CGCM simulations and the other simulations used here are summarized in Table 1; the simulations with "good" age-of-air are identified. The CGCM simulations using the various SSTs are similar but not identical. Results shown below are from specific simulations, but the same conclusions are drawn from any of the simulations.

2.2. Global Modeling Initiative CTM

[15] *Strahan and Douglass* [2004] and *Douglass et al.* [2004] describe and evaluate the GMI CTM and the simulations used here. This version of the GMI CTM uses the same advection scheme, the same look-up tables for the photolysis calculation and essentially the same photochemical mechanism as the CGCM described above. Horizontal resolution for these simulations is 4° latitude × 5° longitude, with 28 vertical levels from the surface to 0.4 hPa. Individual species are advected separately with the exception of some short-lived radical species, and the photochemical contribution to the individual tendency equations are calculated using SMVGEAR II [*Jacobson*, 1998]. The annual mean age of air and the age spectrum are calculated using "pulse" experiments, in which a pulse of a conserved tracer is emitted and tracked.

[16] There are two GMI simulations that differ only in the input meteorological fields. One set of meteorological fields is taken from a GCM that uses a version of the GEOS-4 GCM dynamical core described above and was developed through a collaboration of NASA with the National Center for Atmospheric Research. The second set of fields is taken from a version of the Goddard Earth Observing System Data Assimilation System (GEOS-DAS). This version of GEOS-DAS uses this same GCM in the assimilation process. *Strahan and Douglass* [2004] and *Douglass et al.*

[2004] provide many details about the input meteorological fields and extensive comparisons with observations. The comparisons show that in the upper stratosphere the short-lived radicals such as ClO and NO_2 compare well with observations. However, the overturning circulation associated with this version of GEOS-DAS is much more rapid that that produced by the GCM, and comparisons involving long-lived source gases show that transport produced by the GCM fields is more realistic than that produced using the assimilated meteorology [*Douglass et al.*, 2003]. In the remainder of this paper, simulations using the GMI CTM with meteorological fields from the GCM and GEOS-DAS are referred to as GMI-GCM and GMI-DAS respectively.

2.3. Two-Dimensional CTM

[17] The GSFC two-dimensional (2D) CTM, originally discussed by *Douglass et al.* [1989] and *Jackman et al.* [1990], has undergone steady upgrades and improvements [*Fleming et al.*, 2007, and references therein]. The present version uses changing transport fields over the 1958–2004 period and a climatology for years 2005–2050, all from the National Centers for Environmental Prediction-National Center for Atmospheric Research reanalysis project. *Fleming et al.* [2007] show that long-lived tracers produced using these transport fields compare well with observations. Here the 2D CTM vertical domain extends from the ground to approximately 92 km with levels separated by ~2 km. The horizontal domain extends from pole to pole, with 18 boxes of 10 degrees latitude. The photochemical mechanism includes largely the same reactions as used in the 3D models described above, and also uses kinetic information from the Jet Propulsion Laboratory Evaluation 14 [*Sander et al.*, 2003]. As in the CGCM, a "clock" tracer is included to provide the distributions of the mean age of air.

[18] Simulations using the most recent updated version of the 2D CTM are referred to here as 2D-base. An earlier version of the 2D CTM, the "1995 model" described in *Fleming et al.* [1999, 2001] produces much shorter age-of-air than indicated by measurements. This version of the 2D CTM is referred to as 2D-fast and provides a contrast to the more realistic 2D-base version.

2.4. Trajectory Model

[19] *Schoeberl et al.* [2000, hereafter S2000] describe the 2D trajectory model in detail. The trajectory model uses the residual circulation and mixing coefficients of the 2D CTM. The residual circulation is computed from diabatic heating rates, and the trajectory model scrambles vertical and horizontal positions to simulate mixing [*Feller*, 1968]. S2000 show that the parcel spectra produced by long simulations using a 3D trajectory model are similar to those produced by this 2D model. The 2D trajectory model is used because it is more than 100 times faster than an equivalent 3D calculation.

3. Simulation Results

[20] Simulated fields for the present and near past can be compared with data from various sources to evaluate the representation of the atmosphere by the model. Here we make some comparisons with observations in order to assess the potential uncertainties in simulations of future ozone behavior and contrast results from different simulations.

3.1. Loss Rate Distributions

[21] The annual average local lifetimes (inverse of the local chemical loss frequency) for $CFCl_3$ and CF_2Cl_2 are calculated using CGCM simulated ozone for 2000 and shown in Figure 1. The shading emphasizes the narrow transition separating a region with a lifetime of 2 years or longer from a region with lifetimes of a few months or less. For $CFCl_3$ (CF_2Cl_2) parcels below 50 hPa (20 hPa) outside the tropics have local lifetimes of 2 years or longer. Air parcels that remain below the shaded transition region retain most of their $CFCl_3$ (CF_2Cl_2) while those that go above the transition have their $CFCl_3$ (CF_2Cl_2) rapidly converted to Cl_y.

[22] We compare results from the five simulations with the models described in Section 2 to demonstrate the relationship of the circulation to the loss rates and time-evolving burden of chlorofluorocarbons. The annual-averaged loss distributions (molecules $cm^{-3}s^{-1}$) for each of the simulations are shown for $CFCl_3$ and CF_2Cl_2 for the year 2000 in Figure 2. For $CFCl_3$ most of the loss takes place in the tropics below 10 hPa. There is no significant loss above 10 hPa because destruction below is sufficiently rapid that $CFCl_3$ is destroyed before parcels reach that level. Parcels between 10 and 30 hPa at middle latitudes are similarly depleted of $CFCl_3$ so there is little loss in spite of short chemical lifetimes. Parcels in the lower stratosphere middle latitudes contribute little to the loss because the destruction rate is slow. A similar discussion applies to the loss distributions for CF_2Cl_2, but the region of the greatest loss is found at a higher altitude as expected from the difference in local lifetimes (Figure 1).

[23] It is clear from Figure 2 that the simulations with faster circulations (GMI-DAS and 2D-fast) have larger total loss rates than the CGCM, GMI-GCM and 2D-base. Stronger upwelling shifts the tropical constituent profiles upward and the loss, the product of the mixing ratio and the destruction rate, is commensurately greater.

3.2. Age of Air and Cl_y Distributions

[24] Circulation differences among the models are also apparent through comparison of the stratospheric age-of-air derived from the simulations. These differences can be evaluated by comparison to observations [*Boering et al.*, 1996] as in Figure 3. The values produced by the CGCM, 2D-base and GMI-GCM fall within the 2σ limits of values derived from observations poleward of about 15° latitude. There is a small offset in the tropics, where upward vertical transport and small in-mixing from the middle latitudes both contribute to the mean age [*Waugh and Hall*, 2002]. The 2D-fast and GMI-DAS simulations both produce age distributions that are young compared with the values derived from observations, and could both be described as having fast circulations. The other three could be said to have realistic (slow) circulations. In addition to stronger upwelling, mass continuity requires that models with faster circulations have greater tropical outflow than models with slower circulations.

[25] An important test of the circulation and its interaction with photochemical destruction is provided by the fractional release of chlorine from CFCs. In the upper stratosphere, $CFCl_3$ and CF_2Cl_2 are nearly completely photolyzed in all simulations, and Cl_y time series from different simulations are nearly identical, as shown by time series for GMI-GCM and GMI-DAS at 2°N and 1.3 hPa in Figure 4a. The Cl_y distributions are quite different in the two simulations below

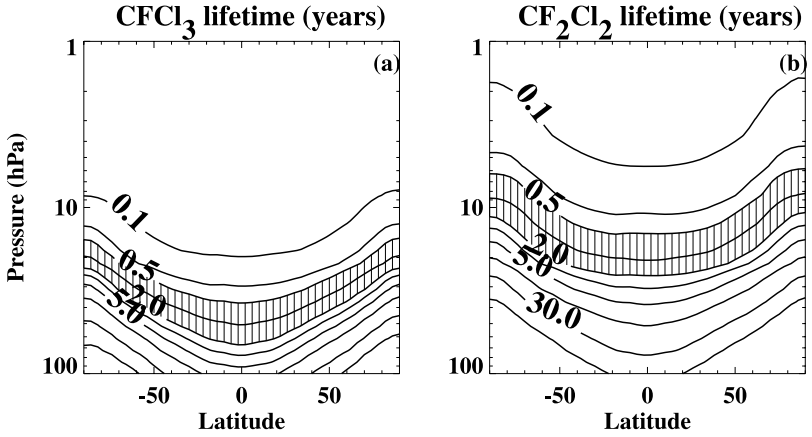

Figure 1. (a) Annual average local lifetimes, calculated using CGCM simulated ozone for 2000, as functions of latitude and altitude (pressure) for $CFCl_3$; (b) same as Figure 1a for CF_2Cl_2.

10 hPa with significantly lower values of Cl_y in GMI-DAS compared with GMI-GCM as shown for annually averaged Cl_y in Figure 4b. The mid and high latitude differences are due to greater horizontal outflow of tropical air that has not experienced ODS destruction in GMI-DAS compared with GMI-GCM, and are larger than 10 percent for most of the region between 70 and 10 hPa, and are larger than 30% in much of the southern hemisphere (Figure 4c). We test the realism of the "fast" versus the "slow" circulation using aircraft observations of $CFCl_3$ and CF_2Cl_2.

3.3. Fractional Release

[26] *Schauffler et al.* [2003] use aircraft observations of various long-lived source gases to compute the fractional release (fr)

$$\mathrm{fr} = (1 - \chi(\mathbf{x})/\chi_i)$$

where $\chi(\mathbf{x})$ is the mixing ratio of a chlorofluorocarbon in a parcel at location **x** (latitude, altitude, pressure, time) and χ_i is the mixing ratio that the parcel would have had if no loss had occurred. We estimate χ_i using the mean age to determine the constituent mixing ratio at the time of entry at the tropical tropopause (i.e., the time of the measurement of χ minus the mean age). We tested this approximation by comparing the mean of the distribution of initial mixing ratios calculated from the constituent time series at the tropical tropopause using the GMI age spectra with χ_i using the calculated mean age. The age spectra are not symmetric and have a tail of elements corresponding to older ages. Each element j is associated with a different entry value χ_i^j because the CFCs are increasing with time. The means of the initial values associated with each element in the age spectrum are only a few percent smaller than values χ_i calculated using the mean age.

[27] *Schauffler et al.* [2003] find a compact relationship between mean age of air and the fractional release in the lower stratosphere using observations from several aircraft campaigns. The simulations considered here produce compact relationships for $CFCl_3$ and CF_2Cl_2 at ~50 hPa (a comparable height to the observations). The simulated values for year 2000 northern hemisphere between 70 and 50 hPa are shown in Figure 5 along with the fractional

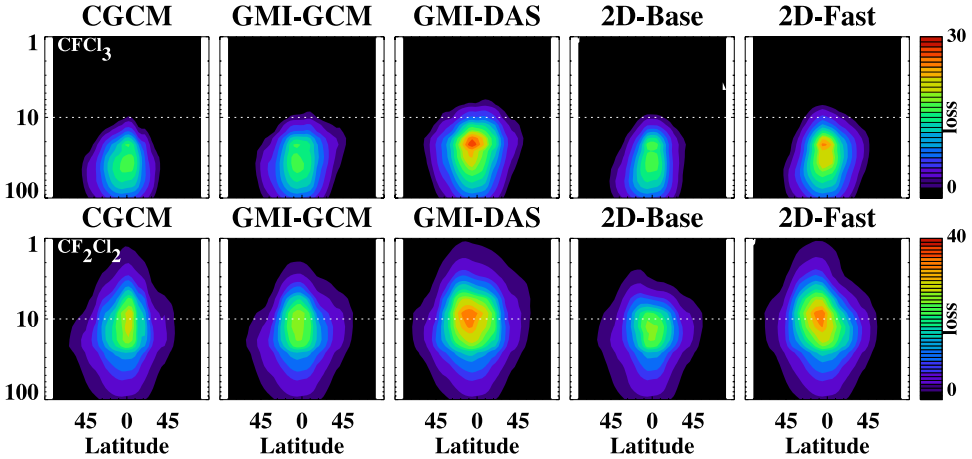

Figure 2. Annual average loss rates (#/cm^3/s) for $CFCl_3$ (top) and CF_2Cl_2 (bottom) as functions of latitude and altitude. Results are shown for five separate simulations indicated by the titles. The white dashed line is the 10 hPa level. The white solid line shows where the local lifetime is 1 year. In the tropics the maximum loss is just above this threshold.

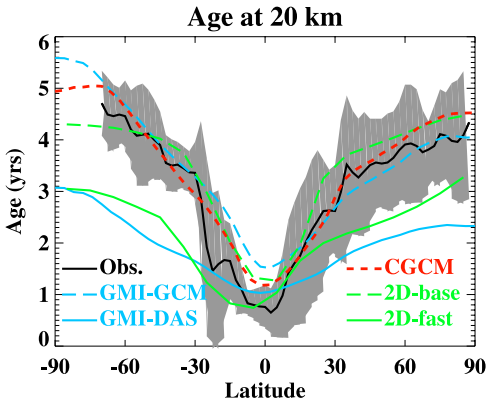

Figure 3. Age-of-air in the lower stratosphere from five simulations compared to values derived from observations (shaded area) [*Boering et al.*, 1996]. The CGCM, 2D-base and GMI-GCM produce a distribution for the age of air that is similar to that observed; the GMI-DAS and 2D-fast ages are too young.

releases and mean ages derived from observations by *Schauffler et al.* [2003]. For CGCM, values are shown for all longitudes and the month March, but the same relationship is found in all months. Annual mean values are shown for the 2D and GMI simulations. For observations and for all simulations, fractional release increases monotonically with age. Simulations using the slower circulations (CGCM, GMI-GCM and 2D-Base), with realistic values for mean age-of air (Figure 3), produce relationships between mean age and fractional release similar to those derived from observations. The fractional releases of both compounds are somewhat larger than observed for air masses with older mean age, with larger differences for CF_2Cl_2. The fast circulations (GMI-DAS and 2D-fast) produce relationships that are clearly separated from those derived from observations or produced by the other simulations (Figure 5).

[28] The ranges of values are somewhat smaller for the GMI simulations than for any of the other simulations. The annual zonal mean age is determined for both GMI simulations using "pulse" experiments; this is plotted versus the fractional release calculated from annual zonal mean tracer fields. The mean age for CGCM is calculated using a "clock" tracer, and its seasonal and longitudinal variations are matched with similar variations in tracer fields. The ranges of age and fractional release using annually zonal averaged fields are reduced by the temporal and spatial averaging but the relationship between them is similar to that obtained with the other simulations.

3.4. Budgets for $CFCl_3$ and CF_2Cl_2

[29] The rate of change of the globally integrated amount of a particular CFC (i.e., the burden B) satisfies a conservation equation

$$\partial B/\partial t = F - B/\tau \quad (1)$$

where τ, the atmospheric lifetime of that CFC, is the globally integrated burden divided by the loss rate. For fixed mixing ratio boundary conditions (as used in all our simulations) the flux F is the number of molecules that must be added to or subtracted from the lowest model layer so that the mixing ratio in that layer follows the imposed mixing ratio time series. Because the mass of the stratosphere is small and the entire troposphere responds rapidly to the boundary conditions, the total atmospheric burdens of $CFCl_3$ or CF_2Cl_2 and the year-to-year changes in the atmospheric burden are largely governed by the boundary conditions. The annual-averaged atmospheric losses (B/τ) for $CFCl_3$ and CF_2Cl_2 as functions of time for the recent past and the future are compared in Figure 6 for each of the five simulations. The integrated loss is much higher for each of the two simulations with fast circulations throughout their respective periods of integration. The simulations with different losses maintain balance between the annual change in burden ($\partial B/\partial t$), the annual loss terms B/τ and the input to the atmosphere with different implied fluxes of $CFCl_3$ and CF_2Cl_2 at the lower boundary. Equation 1 can be solved for the flux necessary to produce the change in burden that is imposed by the mixing ratio boundary conditions. The net

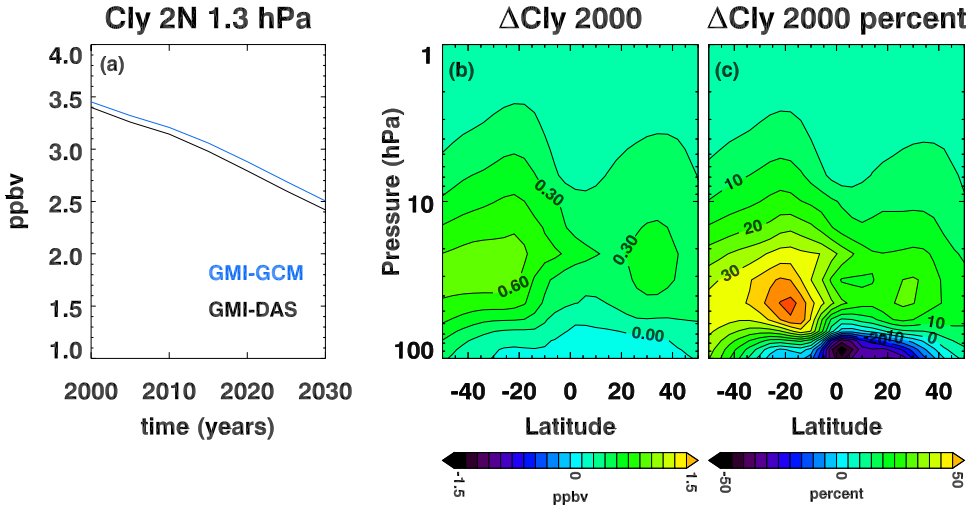

Figure 4. (a) The Cl_y mixing ratios from GMI-GCM (blue) and GMI-DAS (black); (b) annual average difference (ppbv) for the year 2000 $\Delta Cl_y = Cl_y^{GMI\text{-}GCM} - Cl_y^{GMI\text{-}DAS}$; (c) same as Figure 4b in percent.

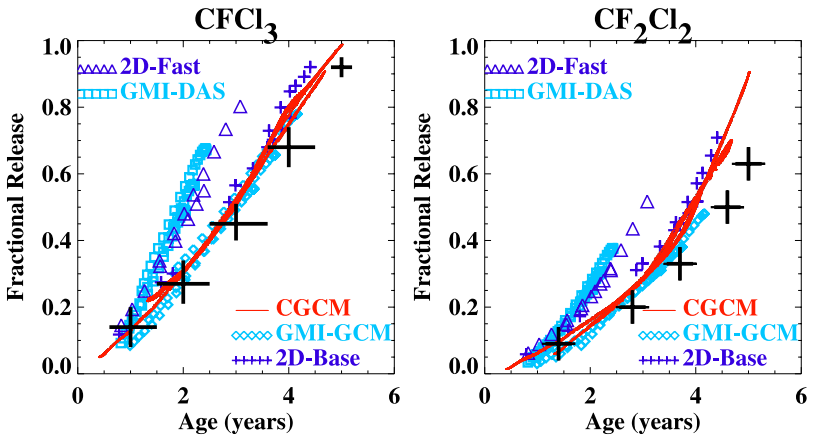

Figure 5. (a) The fractional release of $CFCl_3$ relative to mean age from the simulations, northern hemisphere 50–70 hPa, and the range of values from aircraft observations (large crosses) taken from Figure 7 of *Schauffler et al.* [2003]; (b) same as Figure 5a for CF_2Cl_2.

atmospheric losses up until 2002 for CF_2Cl_2 and $CFCl_3$ from CGCM, 2D-base and 2D-fast (the three simulations that span the appropriate temporal domain) are compared in Table 2. The differences among the simulations are not large compared with the estimated total amount of each CFC that is input to the atmosphere up until 2002 as shown by the last column which is the difference between the loss from 2D-fast (greatest loss) and the loss from CGCM (smallest loss) divided by the estimated total input.

[30] The fluxes inferred from the burden change and simulation losses for the 2D-base and 2D-fast simulations are compared with industrial estimates in Figure 7a for $CFCl_3$ and Figure 7b for CF_2Cl_2. Fluxes were not shown for the GMI simulations as they begin in 1995 when emissions to the atmosphere have already declined substantially from their late 1980s maxima. The CGCM simulations are not shown because they used the mixing ratios recorded on the CCMVal website at 5-year intervals with a linear interpolation between. This does not alter any of the results presented here, but the deduced flux has unrealistic jumps at 5-year intervals.

[31] Up until about 1990 the emissions of CFCs increase rapidly and the change in burden ($\partial B/\partial t$) is significantly larger than the photochemical loss for a given year ($\partial B/\partial t \gg B/\tau$, so $\partial B/\partial t \approx F$), thus differences in the simulated loss rates lead to small percentage differences in the deduced flux. In later years, as $\partial B/\partial t$ decreases, the model differences in the total loss rates lead to a larger percentage difference in the fluxes deduced for the fast and realistic simulations. The $CFCl_3$ flux computed with 2D base is consistently smaller than the bottom-up estimate of emissions [*McCulloch et al.*, 2001]. The 2D base CF_2Cl_2 flux is also smaller than the bottom-up estimate [*McCulloch et al.*, 2003], but the discrepancy is smaller. We infer from differences in the losses in Figure 6 that the CGCM flux for CF_2Cl_2 would be closer to the data while that for $CFCl_3$ would be in worse agreement. This inconsistency for $CFCl_3$ but not for CF_2Cl_2 is similar to results obtained by *Gupta et al.* [2001], who used a three-dimensional model to compute surface mixing ratios using estimated atmospheric release of $CFCl_3$ and CF_2Cl_2 reported through 1996 [*AFEAS*, 1997], including a projection of emissions from nonreporting nations [*Kaye et al.*, 1994]. They found that computed surface mixing ratios exceeded observations for $CFCl_3$ but not CF_2Cl_2 and suggest that the $CFCl_3$ emissions are too large. The CFC lifetimes produced by the model used by *Gupta et al.* [2001] are similar to those produced by the CGCM.

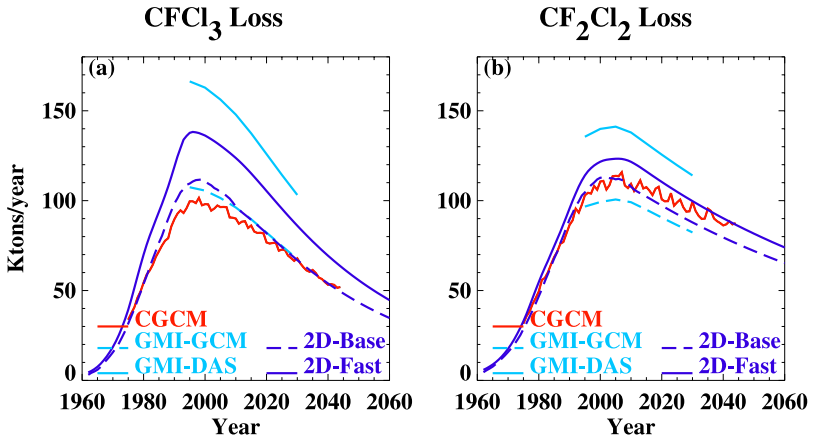

Figure 6. Annual-average loss for 1960–2060 for five simulations for (a) $CFCl_3$ and (b) CF_2Cl_2.

Table 2. Net Atmospheric Losses Up Until 2002 (in Kilotons)

	CGCM	2D-Base	2D-Fast	ΔLoss/(Total Input)
$CFCl_3$	2310	2630	3200	0.10
CF_2Cl_2	2340	2480	2730	0.03

[32] The differences in the losses are also significant in the later years, after ~2020, when the input of CFCs to the atmosphere is expected to be negligible (i.e., F ≈ 0). We compare the fluxes inferred from the burden change and the simulated losses for 2000–2050 in the bottom panels of Figure 8. The GMI-DAS circulation has by far the greatest annual loss of $CFCl_3$ and CF_2Cl_2 (light blue dashed-dotted line in Figure 6) and the inferred fluxes are much greater than the expected zero value. For the three simulations with realistic age of air (CGCM, GMI-GCM and 2D-base) the simulated loss of $CFCl_3$ is less than that required for consistency with the annual change in atmospheric burden, so the inferred fluxes are negative. Negative flux means that the $CFCl_3$ is being removed from the atmosphere by processes other than the stratospheric losses, i.e., the mixing ratio boundary condition creates an artificial surface loss. For the CGCM simulations the negative flux of $CFCl_3$ is about 20% of stratospheric loss after 2020. If we implemented flux boundary conditions in the CGCM, the burden of $CFCl_3$ would decline more slowly than presently forecast.

[33] The annual change in burden is generally better matched by the computed losses for CF_2Cl_2. As for $CFCl_3$, GMI-DAS requires a significant positive flux to maintain consistency with the CF_2Cl_2 burden. A small positive flux is calculated for 2D-fast. The magnitudes of the inferred fluxes calculated for the CGCM (2 cases), GMI-GCM and 2D-base are small compared to the annual loss, i.e., the absolute value of the ratio of the inferred flux to the annual loss is less than 0.05.

[34] We compare the lifetimes (τ = model global burden / model global loss rate) that are calculated for the two CGCM simulations, GMI-GCM, 2D-base, GMI-DAS and 2D-fast in the top two panels of Figure 8. The $CFCl_3$ lifetimes ~2005 are substantially longer than the 45 year lifetime used in recent WMO assessments to produce the mixing ratio scenarios used by CGCM, GMI-GCM and 2D-base. The lifetime range for the models with a realistic relationship between age-of-air and fractional release, 56–61 years, should be compared with the uncertainty range for the $CFCl_3$ lifetime (35–57 years) given in WMO2007 and the lifetime of 45 years used to predict future mixing ratios in Chapter 8 of WMO2007. The range of 56–61 years is outside the observationally derived range of 41 ± 12 years reported by *Volk et al.* [1997]; the quoted uncertainly of 12 years is one-sigma. The 2D-fast lifetime is the same value as used in assessments; the GMI-DAS lifetime is smaller but within the range derived by *Volk et al.* [1997]. The CF_2Cl_2 lifetime for GMI-DAS (80 years) is close to the middle of the range derived by *Volk et al.* [1997], and is shorter than the lifetime used in assessments (100 years). The other simulations produce CF_2Cl_2 lifetimes within 10% of the lifetime used in the assessments.

[35] The lifetimes in the CGCM simulations decrease with time throughout the integration because the overturning circulation speeds up, a common feature of this sort of model [*Butchart et al.*, 2006]. This will be discussed in section 6.

4. Relationship Between Mean Age-of-Air and Fractional Release

[36] In order to understand the relationship between the mean age-of-air and the fractional release (Figure 5), we have calculated age spectra using the 2D trajectory model following the approach of S2000. Five-year back trajectory histories are calculated for 2000 parcels originally located within 0.5° latitude and 0.25 km of 55N, 21 km. This location is chosen to illustrate the relationships; other locations in the lower stratosphere extratropics behave similarly. To avoid confusion between the 2000 parcels for which we calculate back trajectories and the single "parcel" at 55N, 21 km wherein we make hypothetical "measurements," we refer to each of the 2000 parcels as elements of the age spectrum. The age spectrum produced by this calculation is shown in Figure 9a. The time when the

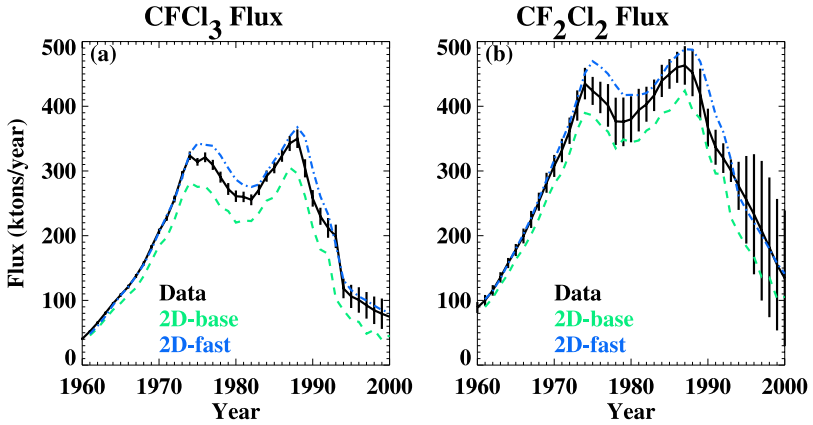

Figure 7. (a) Computed fluxes of $CFCl_3$ necessary to maintain the mixing ratio boundary conditions applied to the 2D-base and 2D-fast simulations. The $CFCl_3$ data are the bottom up estimates of *McCulloch et al.* [2001]; (b) same as Figure 7a for CF_2Cl_2. The CF_2Cl_2 data are taken from *McCulloch et al.* [2003].

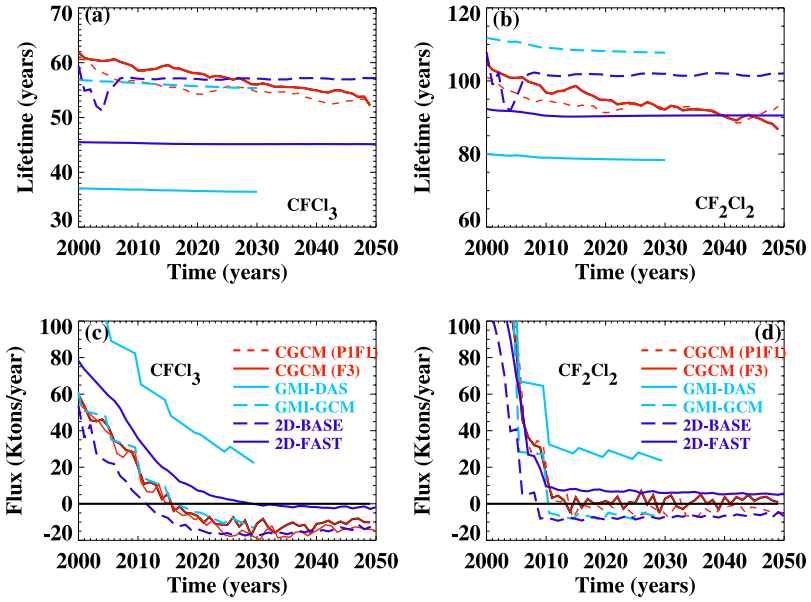

Figure 8. (a) Lifetime of $CFCl_3$ calculated internally from the five simulations; (b) same as Figure 8a for CF_2Cl_2; (c) annual fluxes of $CFCl_3$ implied by the annual change in the atmospheric burden and annual loss for the five simulations; (d) same as Figure 8c for CF_2Cl_2.

each element crosses the tropical tropopause is its age – fewer than 1% of the 2000 parcels fail to cross the tropical tropopause during the integration. The back trajectories of these elements place them in the upper stratosphere, where they experience large horizontal excursions with little change in altitude and they are assigned an age of 5 years. The old age tail is obviously truncated by this approach, but resolving the tail would require thousands of elements and a much longer period of integration without impacting the results as will be clear from the discussion below.

[37] The fractional releases of $CFCl_3$ and CF_2Cl_2 are calculated for each element using an annual mean loss rate. For each element an entry value for each CFC mixing ratio is calculated at the tropical tropopause using the time series of tropospheric mixing ratios and the age of the element. The amount of CFC remaining in each element is calculated by integrating forward from the tropical tropopause along the trajectories, interpolating the annual mean loss to the location of the element at each time step. The distributions of fractional release are given in Figure 9b for $CFCl_3$ and 9c for CF_2Cl_2. The fraction of elements is shown on a log scale for $CFCl_3$ and CF_2Cl_2 to show that there are a few elements that have lost most of their CF_2Cl_2. About 12% of the 2000 elements have lost more than 90% of their $CFCl_3$; only 1% of the elements have lost a comparable fraction of CF_2Cl_2.

[38] The relationship between the fractional release and the age spectrum is not obvious from the distributions shown in Figure 9. The relationship is clarified somewhat by plotting the fractional releases and the maximum altitudes experienced along the trajectories as functions of the age of the elements as shown in Figure 10.

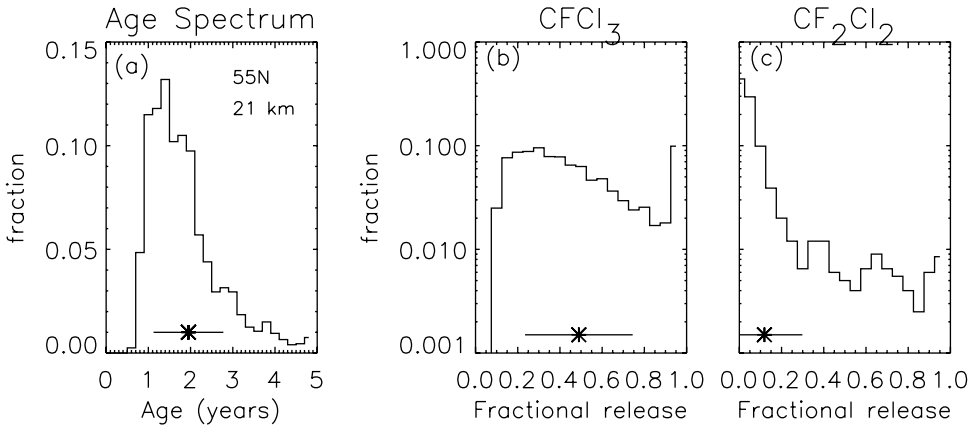

Figure 9. (a) The age spectrum calculated using back trajectories from 55°N, 21 km; (b) the distribution of fractional release values for $CFCl_3$ calculated for the elements of the age spectrum; (c) same as Figure 9b for CF_2Cl_2. On each panel the asterisk is the mean value and the line is the standard deviation of the mean.

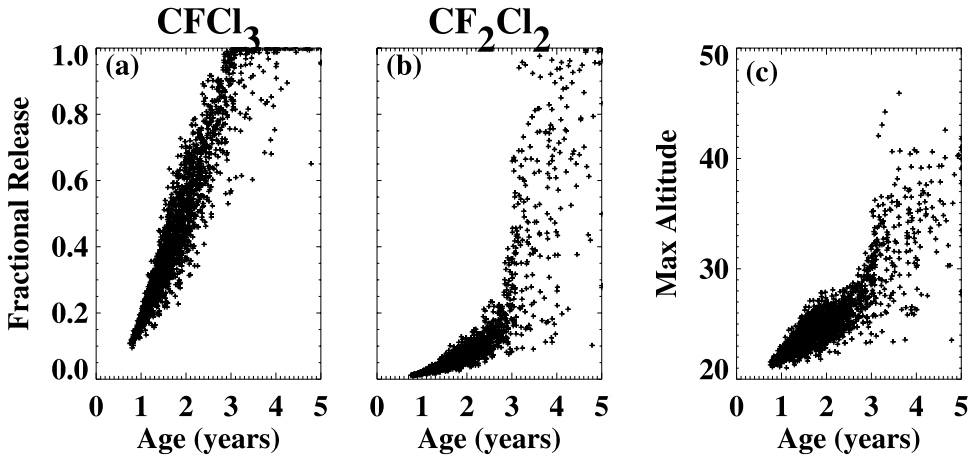

Figure 10. (a) The fractional release of $CFCl_3$ computed using back trajectories for each elements in the age spectrum; (b) same as Figure 10a for CF_2Cl_2; (c) the maximum altitude along the trajectory for each element in the age spectrum.

[39] For $CFCl_3$ (Figure 10a) the relationship between the age of the element and fractional release is fairly compact and linear for ages less than 1.5 years; 35% of the elements fall in this range. For older ages a much wider range of fractional releases is possible; for ages greater than 3 years 10% of the elements have fractional releases of 0.95 or greater. The maximum loss of CF_2Cl_2 takes place at higher altitude (Figure 2), and this is reflected by Figure 10b. The relationship between fractional release and age is fairly compact and linear for element ages less than 2.5–3 years, but there is little correlation between the fractional release and element age for older ages. The relationship between the age of the element and the maximum altitude is also much more compact for elements younger than 3 years (Figure 10c). This result is consistent with the findings of *Hall* [2000] who also studied the maximum altitude distribution of elements of the age spectrum.

[40] S2000 present a conceptual framework for the relationship between the mean age and the tracer amount for long-lived tracers and show that under an average path approximation the tracer amount is more strongly related to the age than to the parcel path. The results of Figure 10 support the relationship between tracer amount and age for younger elements in the age spectrum but behavior is different for the older elements. We explore this result further by plotting the fractional release as a function of the maximum altitude experienced by the element (Figure 11). There is a compact relationship between the fractional release for each element and its maximum altitude for both CFCs. Elements with maximum altitudes greater than 30 km experience virtually complete loss of $CFCl_3$ and are insensitive to further increases in maximum altitude. For CF_2Cl_2 the fractional release continues to increase with increasing maximum altitude because the local loss rate at the maximum altitude is still not fast enough to guarantee complete destruction of the CF_2Cl_2.

[41] To clarify the relationship between the age of the elements and the maximum height, we bin the elements according to their ages (0–1 a, 1–2 a, etc.) and compute the mean and standard deviation of the age and the associated maximum heights. These are shown in Figure 12. Elements associated with older age intervals experience a much

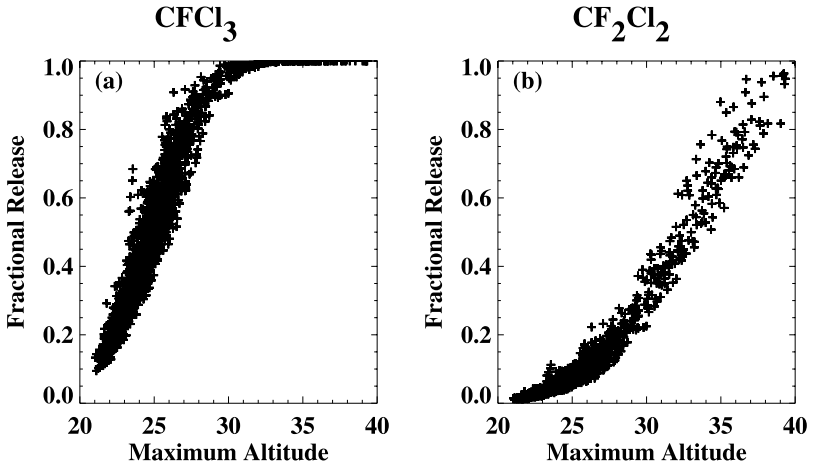

Figure 11. (a) The fractional release of $CFCl_3$ as a function of the maximum altitude along the trajectory; (b) same as Figure 11a for CF_2Cl_2.

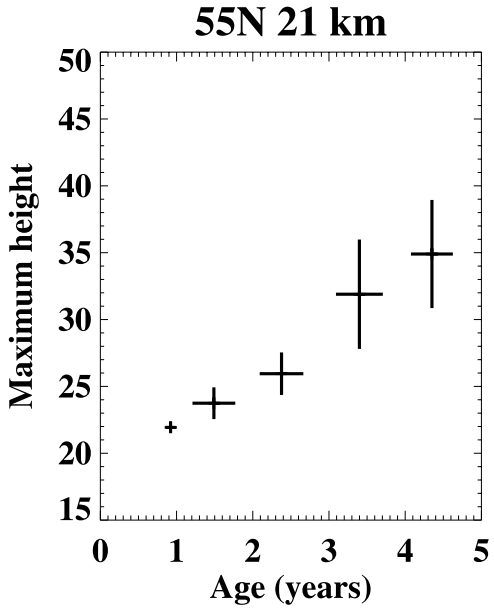

Figure 12. Mean maximum height and mean age for elements that are binned by age in single year intervals. The vertical and horizontal lines show the standard deviation of the maximum height and age respectively.

broader range of maximum heights than those with younger ones as was found by *Hall* [2000]. Also note that elements with ages younger than 3 years have fractional release values for CF_2Cl_2 less than 0.2 (Figure 10b), consistent with the result that the elements rarely if ever rise above 30 km and thus do not experience appreciable destruction of CF_2Cl_2. This analysis shows that a significant fraction of the air in the lower stratosphere with mean age greater than a few years and fractional releases of CF_2Cl_2 greater than 0.4 as reported by *Schauffler et al.* [2003] has at some time experienced heights above 30 km.

[42] The simulated fractional release values for CF_2Cl_2 and $CFCl_3$ from the two simulations with fast circulations (GMI-DAS and 2D-fast) are greater for younger ages than those calculated with the slower circulations. These values

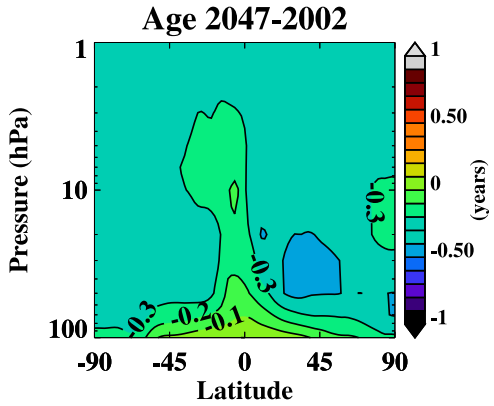

Figure 13. Annual average age-of air is younger in 2047 than 2002 throughout the stratosphere as shown by the difference between five-year averages centered on 2047 and 2002.

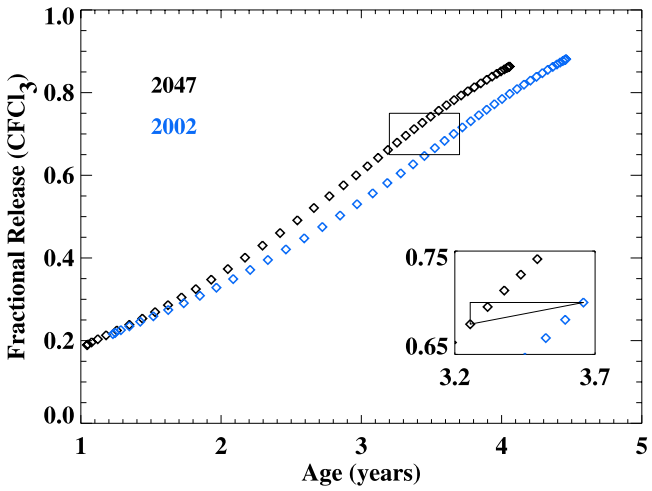

Figure 14. Relationship between mean age and fractional release changes as the residual circulation speeds up. The inset box magnifies the small unlabeled box to compare the change in age (x axis) with the change in fractional release (y axis) for 50°N, 50 hPa.

are also greater than observed. This result makes sense in the context of the trajectory calculations. The elements in the age spectra for the faster circulations must be associated with higher maximum altitudes than elements with similar ages from the age spectra for the slower circulations, thus more CFCs are destroyed annually in simulations with fast circulations even though their residence time in the stratosphere is reduced due to the more rapidly overturning circulation.

5. Future Age and Fractional Release Distributions

[43] As noted above, the lifetimes of $CFCl_3$ and CF_2Cl_2 calculated for CGCM simulations decrease with time as the CGCM integrations progress (Figure 8). This decrease due to circulation change dominates any small increase in lifetime that could result from reduced loss as a result of ozone increases due to recovery from CFCs and stratospheric cooling due to climate change. *Austin and Li* [2006] show that the mean age decreases as the strength of the overturning circulation increases using a similar CCM. The CGCM mean age decreases globally throughout the simulation; the difference in the zonal mean age between 2002 and 2047 is shown in Figure 13 for one simulation; all simulations show similar patterns. In the lower stratosphere the fractional release and mean age exhibit a compact relationship (Figure 5). Figure 14 shows 5-year averages of the annual mean values of the mean age and fractional release for two periods centered on 2002 and 2047. The compact relationships in Figure 14 differ for the two periods because the mean age is more sensitive to the simulated change in circulation than the fractional release. The mean age decreases everywhere in the stratosphere (Figure 13), but the fractional release can decrease, remain nearly constant, or can increase. We emphasize this point by computing the change in fractional release 5-year means centered on 2002 and 2047 in two ways. The changes for

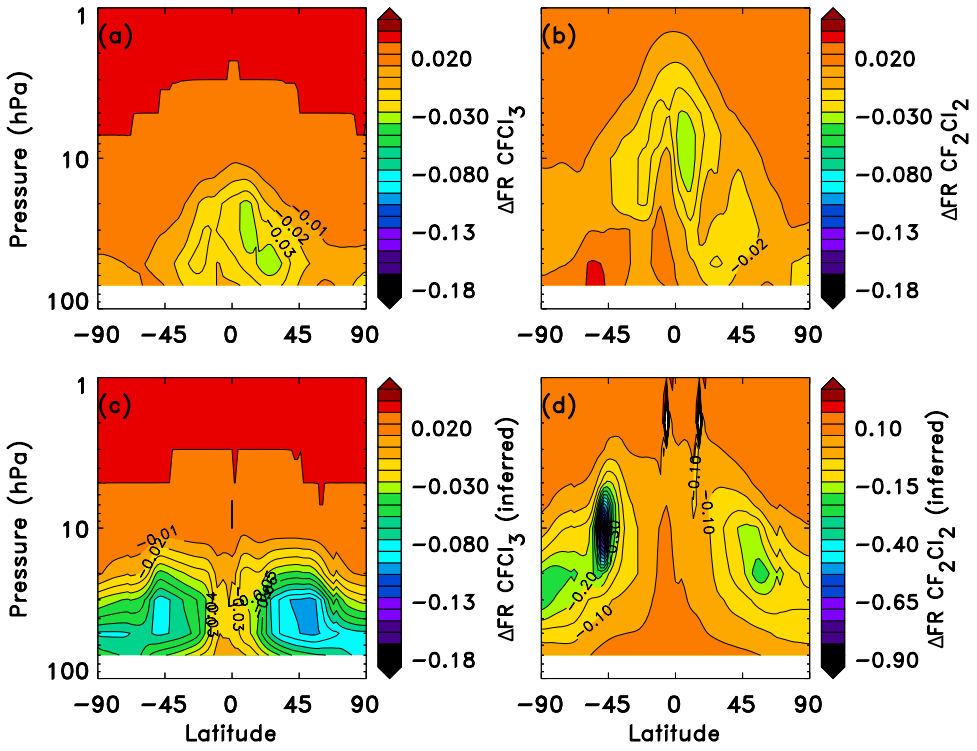

Figure 15. (a) Changes in the fractional release distributions in comparing year 2047 with 2002 for $CFCl_3$ as the circulation speeds up; (b) same as Figure 15a for CF_2Cl_2. (c) Change in fractional release if the 2002 relationship between $CFCl_3$ and mean age is unchanged; (d) same as Figure 15c but for CF_2Cl_2.

$CFCl_3$ and CF_2Cl_2 are given in Figures 15a and 15b. The fractional release values for both constituents decrease slightly in the tropics due to increased upwelling. The maximum decrease in CF_2Cl_2 is found at a higher altitude than that of $CFCl_3$. Figures 15c and 15d show the change for the same time period that would be obtained assuming a fixed relationship between fractional release and mean age. Note that the changes are much larger for Figures 15c and 15d, and the scales also differ. Similar patterns are obtained for all CGCM simulations.

[44] As shown in Figure 13, the mean age becomes younger throughout the stratosphere between 2002 and 2045; the largest changes are found at middle and high latitudes in the lower stratosphere. The patterns of change in fractional releases for $CFCl_3$ and CF_2Cl_2 in Figures 15a and 15b are consistent with the change in the circulation. In the tropics parcels are transported upward more rapidly. Tracer profiles are displaced upward slightly leading to increased loss, but the fractional releases decrease due to a shorter residence time. The largest decrease in the fractional release of $CFCl_3$ is seen in the region of maximum loss, i.e., between 50 and 30 hPa (Figure 2 and Figure 15a). For CF_2Cl_2 the largest decrease in fractional release is between 20 and 5 hPa (Figure 2 and Figure 15b). Outside the tropics the fractional release changes very little as the mean age decreases, suggesting that although some elements in the age spectrum experience higher maximum heights and greater loss, this is balanced by the overall shift in the age spectrum toward younger ages. The shift in the relationship between the mean age and the fractional release as the circulation speeds up is explained by the relationships between the age spectrum, the maximum height, and the fractional release explored in the previous section. Figures 15c and 15d assume that the relationships between the fractional releases and the mean ages are unchanged, and show a completely different pattern from that produced by the CGCM simulations. Under this assumption, the fractional release would always decrease as the age decreases. The largest changes would occur in the middle high latitude lower stratosphere, the opposite of what is produced by the simulations.

6. Discussion and Conclusions

[45] In all current ozone assessments, ODS mixing ratios are specified as model boundary conditions. The use of these mixing ratio boundary conditions guarantees that the tropospheric mixing ratios match observations. Even so, the amount of inorganic chlorine in the lower stratosphere varies significantly among simulations because the loss rates of the chlorofluorocarbons vary for different circulations.

[46] The trajectory analysis shows how the mean age and the fractional release are related through the age spectrum. Together, comparison of the simulated mean age and the fractional release of an ODS in the lower stratosphere with observed values test the integrated loss and thereby tests the simulated lifetime. Although the mean age and the fractional release both depend on the strength of the overturning circulation, both also depend on other factors such as horizontal mixing between the tropics and middle latitudes. It is possible for a simulation to produce a credible distribution for mean age and fail to produce a realistic distribution for Cl_y [*Waugh et al.*, 2007]. The $CFCl_3$ lifetime for the

simulations that have realistic age-of-air and reproduce the observed relationship between the mean age and the fractional release is 56–64 years, outside the range derived from observations (41 ± 12 years) reported by *Volk et al.* [1997]. The range of 56–64 years should be compared with the 35–57 year range and 45 year lifetime used to predict future mixing in WMO2007. Future evaluations of ODS lifetimes from a suite of atmospheric models should include comparisons of both mean age and fractional release to interpret differences among models.

[47] There are several advantages to the use of flux boundary conditions. First, the simulated ODS evolution would always be consistent with simulated loss. Second, use of flux boundary conditions would remove the constraint on the time dependence of simulated Cl_y and chlorine containing species. The modeled mixing ratios of Cl_y and HCl in the upper atmosphere are largely controlled by the mixing ratio boundary conditions; the exact timing of the maxima will vary if the times to propagate the boundary conditions to the upper atmosphere differ. The amount of Cl_y in the lower stratosphere is strongly influenced by differences in circulation among various simulations. If flux boundary conditions were used the level of Cl_y in the upper stratosphere and its rate of increase and decline would also vary depending on the simulation circulation and transport through their impact on the loss rate, and comparisons with time series would provide additional information about model performance. For example, *Lary et al.* [2007] have combined measurements of various chlorine species to produce a global estimate of Cl_y for 1991–2006. *Froidevaux et al.* [2006] demonstrate that upper stratospheric chlorine decreased between July 2004 and December 2005.

[48] The question of the amount of chlorofluorocarbons that is presently "banked" and the rate of release to the atmosphere is difficult to address. Top-down and bottom-up estimates differ, thus the projections for future atmospheric levels of CFCs are uncertain. We find that the magnitude of the fluxes needed to maintain the mixing ratio boundary conditions in our simulations depends on the overall vigor of the atmospheric circulation. Comparisons with observations presented by *Pawson et al.* [2008] as well as the comparisons with age-of-air and fractional release shown here indicate that the circulations and destruction rates of CGCM, GMI-GCM and 2D-base are more realistic than those of GMI-DAS and 2D-fast. An important implication of these results is that simulations with realistic age-of-air and fractional release of chlorine yield longer atmospheric lifetimes for chlorofluorocarbons. The effect is greater for $CFCl_3$ (56 years versus 45 years) than for CF_2Cl_2 (101–110 years versus 100 years). The difference in the loss estimates is comparable to the difference in the bank estimates for the "bottom up" and "top down" evaluations reported by *Daniel et al.* [2007]. If these longer lifetimes are more appropriate, the amounts of $CFCl_3$ and CF_2Cl_2 stored in banks estimated from top-down calculations would increase and agree better with the bottom-up estimates. Finally, we find that the lifetime decreases as the circulation speeds up due to climate change as in most CCM calculations. Flux boundary conditions for long-lived gases must be used to test whether the change in the loss due to the circulation speed-up has a significant impact on the decline of CFCs in the atmosphere.

[49] **Acknowledgments.** This work was supported by NASA's Atmospheric Chemistry and Analysis Program (ACMAP) and by the Modeling, Analysis and Prediction (MAP) Program. CGCM results were generated using NASA's Columbia supercomputer housed at the NASA Ames Research Center. This is contribution No. 3 of the Goddard Chemistry/Climate Modeling Project.

References

Alternative Fluorocarbons Environmental Acceptability Study (AFEAS) (1997), *Production, Sales and Atmospheric Release of Fluorocarbons Through 1996, Washington, D.C.*

Austin, J., and F. Li (2006), On the relationship between the strength of the Brewer-Dobson circulation and the age of stratospheric air, *Geophys. Res. Lett.*, *33*, L17807, doi:10.1029/2006GL026867.

Boering, K. A., S. C. Wofsy, B. C. Daube, H. R. Schneider, M. Loewenstein, and J. R. Podolske (1996), Stratospheric mean ages and transport rates from observations of carbon dioxide and nitrous oxide, *Science*, *274*(5291), 1340–1343.

Butchart, N., and A. A. Scaife (2001), Removal of chlorofluorcarbons by increased mass exchange between the stratosphere and troposphere in a changing climate, *Nature*, *410*, 799–802.

Butchart, et al. (2006), Simulations of the anthropogenic change in the strength of the Brewer-Dobson circulation, *Clim. Dyn.*, *27*, 727–741.

Considine, D. B., A. R. Douglass, P. S. Connell, D. E. Kinnison, and D. A. Rotman (2000), A polar stratospheric cloud parameterization for the global modeling initiative three-dimensional model and its response to stratospheric aircraft, *J. Geophys. Res.*, *105*, 3955–3973.

Daniel, J. S., G. J. M. Velders, S. Solomon, M. McFarland, and S. A. Montzka (2007), Present and future sources and emissions of halocarbons: Toward new constraints, *J. Geophys. Res.*, *112*, D02301, doi:10.1029/2006JD007275.

Douglass, A. R., and S. R. Kawa (1999), Contrast between 1992 and 1997 high-latitude spring Halogen Occultation Experiment observations of lower stratospheric HCl, *J. Geophys. Res.*, *104*, 18,739–18,754.

Douglass, A. R., C. H. Jackman, and R. S. Stolarski (1989), Comparison of model results transporting the odd nitrogen family with results transporting separate odd nitrogen species, *J. Geophys. Res.*, *94*, 9862–9872.

Douglass, A. R., M. R. Schoeberl, S. R. Kawa, and E. V. Browell (2001), A composite view of ozone evolution in the 1995–1996 northern winter polar vortex developed from airborne lidar and satellite observations, *J. Geophys. Res.*, *106*, 9879–9895.

Douglass, A. R., M. R. Schoeberl, R. B. Rood, and S. Pawson (2003), Evaluation of transport in the lower tropical stratosphere in a global chemistry and transport model, *J. Geophys. Res.*, *108*(D9), 4259, doi:10.1029/2002JD002696.

Douglass, A. R., R. S. Stolarski, S. E. Strahan, and P. S. Connell (2004), Radicals and reservoirs in the GMI chemistry and transport model: Comparison to measurements, *J. Geophys. Res.*, *109*, D16302, doi:10.1029/2004JD004632.

Eyring, V., et al. (2006), Assessment of temperature, trace species, and ozone in chemistry-climate model simulations of the recent past, *J. Geophys. Res.*, *111*, D22308, doi:10.1029/2006JD007327.

Feller, W. (1968), *An Introduction to Probability Theory and Its Applications*, vol. 1, John Wiley, New York.

Fleming, E. L., C. H. Jackman, R. S. Stolarski, and D. B. Considine (1999), Simulation of stratospheric tracers using an improved empirically based two-dimensional model transport formulation, *J. Geophys. Res.*, *104*, 23911–23934.

Fleming, E. L., C. H. Jackman, D. B. Considine, and R. S. Stolarski (2001), Sensitivity of tracers and a stratospheric aircraft perturbation to two-dimensional model transport variations, *J. Geophys. Res.*, *106*, 14,245–14,263.

Fleming, E. L., C. H. Jackman, D. K. Weisenstein, and M. K.W. Ko (2007), The impact of interannual variability on multi-decadal total ozone simulations, *J. Geophys. Res.*, *112*, D10310, doi:10.1029/2006JD007953.

Froidevaux, L., et al. (2006), Temporal decrease in upper atmospheric chlorine, *Geophys. Res. Lett.*, *33*, L23812, doi:10.1029/2006GL027600.

Gupta, M. L., R. P. Turco, C. R. Mechoso, and J. A. Spahr (2001), On-line simulations of passive chemical tracers in the University of California, Los Angeles, atmospheric general circulation model 1, CFC-11 and CFC-12, *J. Geophys. Res.*, *106*, 12,401–12,417.

Hall, T. M. (2000), Path histories and timescales in stratospheric transport: Analysis of an idealized model, *J. Geophys. Res.*, *105*, 22,811–22,823.

Intergovernmental Panel on Climate Change/Technology and Economic Assessment Panel (2005), IPCC *Special Report: Safeguarding the Ozone Layer and the Global Climate System: Issues Related to Hydrofluorocarbons and Perfluorocarbons*, 478 pp., Cambridge Univ. Press, New York.

Jackman, C. H., A. R. Douglass, R. B. Rood, R. D. McPeters, and P. E. Meade (1990), Effect of solar proton events on the middle atmosphere during the past two solar cycles as computed using a two-dimensional model, *J. Geophys. Res.*, *95*, 7417–7428.

Jacobson, M. Z. (1998), Improvement of SMVGEAR II on vector and scalar machines through absolute error tolerance control, *Atmos. Environ.*, *32*, 791–796.

Johns, T. C., et al. (2006), The new Hadley Centre Climate Model (HadGEM1): Evaluation of coupled simulations, *J. Clim.*, *19*, 1327–1353.

Kaye, J. A., S. A. Penkett, and F. M. Ormond (Eds.) (1994), Report on concentrations, lifetimes and trends of CFCs, halons and related species, *NASA Ref. Publ.*, *1339*.

Kiehl, J. T., J. J. Hack, G. B. Bonan, B. A. Boville, D. L. Williamson, and P. J. Rasch (1998), The national center for atmospheric research community climate model: CCM3, *J. Clim.*, *11*, 1131–1149.

Lary, D. J., D. W. Waugh, A. R. Douglass, R. S. Stolarski, P. A. Newman, and H. Mussa (2007), Variations in stratospheric inorganic chlorine between 1991 and 2006, *Geophys. Res. Lett.*, *34*, L21811, doi:10.1029/2007GL030053.

Lin, S.-J. (1997), A finite-volume integration scheme for computing pressure-gradient forces in general vertical coordinates, *Q. J. R. Meteorol. Soc.*, *123*, 1749–1762.

Lin, S.-J., and R. B. Rood (1996), Multidimensional flux form semi-Lagrangian transport schemes, *Mon. Weather Rev.*, *124*, 2040–2070.

Lin, S.-J., and R. B. Rood (1997), An explicit flux-form semi-Lagrangian shallow water model on the sphere, *Q. J. R. Meteorol. Soc.*, *123*, 2448–2477.

Logan, J. A. (1999), An analysis of ozonesonde data for the troposphere: Recommendations for testing 3-D models and development of a gridded climatology for tropospheric ozone, *J. Geophys. Res.*, *104*, 16,115–16,150.

McCulloch, A., P. Ashford, and P. M. Midgley (2001), Historic emissions of fluortrichloromethane (CFC-111) based on a market survey, *Atmos. Environ.*, *35*, 4387–4397.

McCulloch, A., P. M. Midgley, and P. Ashford (2003), Releases of refrigerant gases (CFC-12, HCFC-22 and HFC-134a) to the atmosphere, *Atmos. Environ.*, *37*, 889–902.

Newman, P. A., E. R. Nash, S. R. Kawa, S. A. Montzka, and S. M. Schauffler (2006), When will the Antarctic ozone hole recover, *Geophys. Res. Lett.*, *33*, L12814, doi:10.1029/2005GL025232.

Pawson, S., R. S. Stolarski, A. R. Douglass, P. A. Neuman, J. E. Nielsen, S. M. Frith, and M. L. Gupta (2008), Goddard Earth Observing System chemistry-climate model simulations of stratospheric ozone-temperature coupling between 1950 and 2005, *J. Geophys. Res.*, *113*, D12103, doi:10.1029/2007JD009511.

Rayner, N. A., D. E. Parker, E. B. Horton, C. K. Folland, L. V. Alexander, D. P. Rowell, E. C. Kent, and A. Kaplan (2003), Global analyses of sea surface temperature, sea ice and night marine air temperature since the late nineteenth century, *J. Geophys. Res.*, *108*(D14), 4407, doi:10.1029/2002JD002670.

Sander, S. P., et al. (2003), Chemical kinetics and photochemical data for use in atmospheric studies, Evaluation number 14, JPL Publ. 02–25.

Schauffler, S. M., E. L. Atlas, S. G. Donnelly, A. Andrews, S. A. Montzka, J. W. Elkins, D. F. Hurst, P. A. Romashkin, G. S. Dutton, and V. Stroud (2003), Chlorine budget and partitioning during the Stratospheric Aerosol and Gas Experiment (SAGE) III Ozone Loss and Validation Experiment (SOLVE), *J. Geophys. Res.*, *108*(D5), 4173, doi:10.1029/2001JD002040.

Schoeberl, M. R., L. C. Sparling, C. H. Jackman, and E. L. Fleming (2000), A Lagrangian view of stratospheric trace gas distributions, *J. Geophys. Res.*, *105*, 1537–1552.

Stolarski, R. S., A. R. Douglass, M. Gupta, P. A. Newman, S. Pawson, M. R. Schoeberl, and J. E. Nielsen (2006a), An ozone increase in the Antarctic summer stratosphere: A dynamical response to the ozone hole, *Geophys. Res. Lett.*, *33*, L21805, doi:10.1029/2006GL026820.

Stolarski, R. S., A. R. Douglass, S. Steenrod, and S. Pawson (2006b), Trends in stratospheric ozone: Lessons learned from a 3D chemical transport model, *J. Atmos. Sci.*, *63*, 1028–1041.

Strahan, S. E., and A. R. Douglass (2004), Evaluating the credibility of transport processes in simulations of ozone recovery using the Global Modeling Initiative three-dimensional model, *J. Geophys. Res.*, *109*, D05110, doi:10.1029/2003JD004238.

Volk, C. M., J. W. Elkins, D. W. Fahey, G. S. Dutton, J. M. Gilligan, M. Loewenstein, J. R. Podolski, K. R. Chan, and M. R. Gunson (1997), Evaluation of source gas lifetimes from stratospheric observations, *J. Geophys. Res.*, *102*, 25,543–25,564.

Waugh, D. W., and T. M. Hall (2002), Age of stratospheric air: Theory, observations and models, *Rev. Geophys.*, *40*(4), 1010, doi:10.1029/2000RG000101.

Waugh, D. W., S. E. Strahan, and P. A. Newman (2007), Sensitivity of stratospheric inorganic chlorine to differences in transport, *Atmos. Chem. Phys.*, *7*, 4935–4941.

World Meteorological Organization (WMO) (1985), *Atmospheric Ozone 1985: Assessment of Our Understanding of the Processes Controlling its Present Distribution and Change, Rep. 16*, Global Ozone Res. and Monit. Proj., Geneva.

World Meteorological Organization (WMO) (1999), *Scientific Assessment of Ozone Depletion: 1998*, *Rep. 44*, Global Ozone Res. and Monit. Proj., Geneva.

World Meteorological Organization (WMO) (2003), *Scientific Assessment of Ozone Depletion: 2002, Rep. 47*, Global Ozone Res. and Monit. Proj., Geneva.

World Meteorological Organization (WMO) (2007), *Scientific Assessment of Ozone Depletion: 2006, Rep. 50*, Global Ozone Res. and Monit. Proj., Geneva.

A. R. Douglass, C. H. Jackman, P. A. Newman, M. R. Schoeberl, and R. S. Stolarski, Atmospheric Chemistry and Dynamics Branch, Code 613.3, NASA Goddard Space Flight Center, Greenbelt, MD 20771, USA. (anne.r.douglass@nasa.gov)

E. L. Fleming, Science Systems and Applications, Inc., NASA Goddard Space Flight Center, Code 613.3, Greenbelt, MD 20771, USA.

M. L. Gupta, Federal Aviation Administration, FAA, Office of Environment and Energy, AEE-300 Emissions Division, 800 Independence Avenue, S.W., Washington, DC 20591, USA.

J. E. Nielsen, Global Modeling and Assimilation Office, NASA Goddard Space Flight Center, Code 610.0, Greenbelt, MD 20771, USA.